

ornl

ORNL/TM-10951

**OAK RIDGE
NATIONAL
LABORATORY**

MARTIN MARIETTA

Transition from Resistive Ballooning to Neoclassical Magnetohydrodynamic Pressure-Gradient-Driven Instability

D. A. Spong
K. C. Shaing
B. A. Carreras
L. A. Charlton
J. D. Callen
L. Garcia

OAK RIDGE NATIONAL LABORATORY
CENTRAL RESEARCH LIBRARY
CIRCULATION SECTION
OAK RIDGE, TENN.
LIBRARY LOAN COPY
DO NOT TRANSFER TO ANOTHER PERSON
If you wish someone else to see this
report, send its name with report and
the library will arrange a loan.

OPERATED BY
MARTIN MARIETTA ENERGY SYSTEMS, INC.
FOR THE UNITED STATES
DEPARTMENT OF ENERGY

Printed in the United States of America. Available from
National Technical Information Service
U. S. Department of Commerce
5285 Port Royal Road, Springfield, Virginia 22161
NTIS price codes—Printed Copy: A03; Microfiche A01

This report was prepared as an account of work sponsored by an agency of the United States Government. Neither the United States Government nor any agency thereof, nor any of their employees, makes any warranty, express or implied, or assumes any legal liability or responsibility for the accuracy, completeness, or usefulness of any information, apparatus, product, or process disclosed, or represents that its use would not infringe privately owned rights. Reference herein to any specific commercial product, process, or service by trade name, trademark, manufacturer, or otherwise, does not necessarily constitute or imply its endorsement, recommendation, or favoring by the United States Government or any agency thereof. The views and opinions of authors expressed herein do not necessarily state or reflect those of the United States Government or any agency thereof.

ORNL/TM-10951
Dist. Category UC-427

Fusion Energy Division

**TRANSITION FROM RESISTIVE BALLOONING
TO NEOCLASSICAL MAGNETOHYDRODYNAMIC
PRESSURE-GRADIENT-DRIVEN INSTABILITY**

D. A. Spong
K. C. Shaing
B. A. Carreras
L. A. Charlton

J. D. Callen
University of Wisconsin, Madison, Wisconsin 53706

L. Garcia
Universidad Complutense, Madrid, Spain

Date published: October 1988

Prepared by the
OAK RIDGE NATIONAL LABORATORY
Oak Ridge, Tennessee 37831
operated by
MARTIN MARIETTA ENERGY SYSTEMS, INC.
for the
U.S. DEPARTMENT OF ENERGY
under contract DE-AC05-84OR21400



3 4456 0283144 3

CONTENTS

ABSTRACT	v
I. INTRODUCTION	1
II. TIME-EVOLUTION EQUATIONS AND NUMERICAL METHODS	3
III. NUMERICAL RESULTS	6
IV. CONCLUSIONS AND SUMMARY	10
REFERENCES	12

ABSTRACT

The linearized neoclassical magnetohydrodynamic equations, including perturbed neoclassical flows and currents, have been solved for parameter regimes where the neoclassical pressure-gradient-driven instability becomes important. This instability is driven by the fluctuating bootstrap current term in Ohm's law. It begins to dominate the conventional resistive ballooning mode in the banana-plateau collisionality regime [$\mu_e/\nu_e \sim \sqrt{\epsilon}/(1 + \nu_{*e}) > \epsilon^2$] and is characterized by a larger radial mode width and higher growth rate. The neoclassical instability persists in the absence of the usual magnetic field curvature drive and is not significantly affected by compressibility. Scalings with respect to β , n (toroidal mode number), and μ (neoclassical viscosity) are examined using a large-aspect-ratio, three-dimensional initial-value code that solves linearized equations for the magnetic flux, fluid vorticity, density, and parallel ion flow velocity in axisymmetric toroidal geometry.

I. INTRODUCTION

The fluid moment equation approach developed for neoclassical equilibrium processes¹ has recently been extended to higher-frequency instability phenomena in axisymmetric toroidal plasmas.²⁻⁵ This is of importance for understanding existing and future tokamak plasmas, which operate well into the long mean-free-path regime. These neoclassical magnetohydrodynamic (MHD) equations take into account modifications to plasma flows and currents that result when particles complete at least one toroidal transit before experiencing collisions, in contrast to the usual reduced resistive MHD equations, which are valid only in the Pfirsch-Schlüter regime (multiple collisions per toroidal transit).

The primary features of the new neoclassical MHD equations arise from inclusion of viscous relaxation effects within magnetic flux surfaces. These lead to such effects as (1) a fluctuating bootstrap current in Ohm's law, resulting from the parallel electron viscous damping of the poloidal flow induced by the perturbed radial pressure gradient; (2) a rapid ($\simeq \nu_i$) damping of the poloidal ion flow so that the residual flow is primarily toroidal; and (3) an enhanced (by B^2/B_θ^2) polarization drift and a resulting enhancement of the perpendicular dielectric constant from parallel flow inertia (this causes the equations to depend only on the poloidal magnetic field B_θ). These effects can lead to both substantial modifications of the known resistive MHD instabilities and new instabilities made possible through the additional mechanisms for accessing the sources of free energy that are introduced through the neoclassical terms.

One new instability is the neoclassical pressure-gradient-driven mode,^{2,6,7} which arises from the expansion free energy through the fluctuating bootstrap current term. This instability has been analyzed using both kinetic^{6,7} and fluid moment² approaches and has been predicted to have a growth rate comparable to that of the conventional resistive ballooning mode. Turbulent transport models based on medium-mode-number ($n \lesssim 10$) resistive ballooning modes have been shown to correlate well with experimental data in the Impurity Study Experiment (ISX-B) as the auxiliary heating power (or plasma stored energy) is increased.^{8,9} The similarities of these instabilities to the new pressure-gradient-driven neoclassical instability thus make the latter a strong candidate for anomalous transport models in higher-temperature plasma regimes.

In this paper we extend the previous analytic treatments of the pressure-gradient-driven neoclassical MHD instability by solving recently derived³⁻⁵ neoclassical moment equations for the time evolution of the magnetic flux, fluid vorticity, density, and parallel ion flow velocity. A three-dimensional (3-D), large-aspect-ratio, initial-value code based on the FAR code has been developed.¹⁰ This code solves the linearized moment equations starting from an axisymmetric toroidal equilibrium state. This approach has allowed the inclusion of a number of effects that were either not included in the analytic calculations or not readily apparent in them. First, the compressibility coupling from the density to the ion parallel flow equation is retained. This effect is of interest since it was found to be strongly stabilizing in the case of the resistive ballooning mode⁹ as higher-temperature regimes were considered. Also, we do not assume strong ion poloidal flow damping, as was the case in the simplest analytic models, but solve the ion parallel flow equation consistently with the dynamical evolution of the other variables. Next, we have included the radial and poloidal flows in greater detail than previously considered, since these were necessary to obtain proper behavior of the solutions at the origin. In the analytic calculations, this was not critical because a geometry local to the resonant flux surfaces was employed. The effects of classical viscosity and density diffusion are also considered.

The code has been used to check scalings of the neoclassical instability with toroidal mode number, plasma beta, and neoclassical electron viscosity. By gradually increasing the neoclassical electron viscosity, the transition from a resistive ballooning instability to the neoclassical instability can be followed in detail. Finally, by removing terms, the code has been used to check some of the predictions and assumptions of the analytic treatments, such as the validity of rapid ion poloidal flow damping, the cancellation of the lowest-order geodesic curvature effects by Pfirsch-Schlüter currents, and the lack of explicit dependence of the growth rate on resistivity.

This paper is organized as follows. First, the time evolution equations appropriate for reduced neoclassical MHD are discussed. Next, the numerical initial-value code is described. We then present results demonstrating the transition from a resistive ballooning mode to a neoclassical pressure-gradient-driven mode as the collisional mean free path is increased. Next, the scaling of the neoclassical mode with respect to various quantities is examined. Finally, the effects of removing and adding compressibility, resistivity, curvature ($\hat{b} \cdot \vec{\nabla} p \times \kappa$) drive, and classical viscosity are examined.

II. TIME-EVOLUTION EQUATIONS AND NUMERICAL METHODS

The calculations discussed here are based on the neoclassical moment equations for n , A_{\parallel} , ϕ , and $V_{\parallel i}$. These equations,³⁻⁵ which result from using the electron density continuity equation, Ohm's law coupled with Faraday's induction law, and the perpendicular and parallel ion momentum equations (in mks units), are

$$\frac{\partial n_e}{\partial t} = -\vec{\nabla} \cdot (n_e \vec{v}_{\perp e}) - (\vec{B} \cdot \vec{\nabla}) \left[\frac{n_e}{B} \left(V_{\parallel i} - \frac{J_{\parallel}}{en_e} \right) \right] , \quad (1)$$

$$-\frac{F}{R^2} \frac{\partial \psi}{\partial t} = -\frac{J_{\parallel} B}{\sigma_{\parallel}} - (\vec{B} \cdot \vec{\nabla}) \left(\phi - \frac{T_e}{e} \ln n_e \right) + \frac{1}{en_e} \vec{B} \cdot (\vec{\nabla} \cdot \vec{\Pi}_{\parallel e}) , \quad (2)$$

$$\begin{aligned} \vec{\nabla} \cdot \left[\frac{\rho_m}{B^2} \vec{B} \times \left(\frac{\partial}{\partial t} + \vec{v}_E \cdot \vec{\nabla} \right) \vec{v}_{\perp i} \right] = & -(\vec{B} \cdot \vec{\nabla}) \left(\frac{J_{\parallel}}{B} \right) - \vec{\nabla} \cdot \left(\frac{1}{B^2} \vec{B} \times \vec{\nabla} p \right) \\ & - \vec{\nabla} \cdot \left(\frac{\vec{B} \times \vec{\nabla} \cdot \vec{\Pi}_{\parallel i}}{B^2} \right) , \end{aligned} \quad (3)$$

$$\rho_m \left(\frac{\partial}{\partial t} + \vec{v}_E \cdot \vec{\nabla} \right) (V_{\parallel i} B) = -(\vec{B} \cdot \vec{\nabla}) p - \vec{B} \cdot (\vec{\nabla} \cdot \vec{\Pi}_{\parallel i}) , \quad (4)$$

where n_e is the electron density, ψ is the poloidal magnetic flux, $V_{\parallel i}$ is the parallel ion flow velocity, ϕ is the electric potential,

$$\rho = n_i m_i ,$$

$$F(\psi) \equiv RB_t ,$$

$$\vec{v}_E = \frac{\vec{B}}{B^2} \times \vec{\nabla} \phi ,$$

$$J_{\parallel} = \frac{B}{\mu_0 F} R^2 \vec{\nabla} \cdot (R^{-2} \vec{\nabla} \psi) [1 + \mathcal{O}(\epsilon^2)] = n_e e (V_{\parallel i} - V_{\parallel e}) ,$$

$$\vec{v}_{\perp s} = \frac{\vec{B}}{B^2} \times \vec{\nabla} \left(\phi + \frac{T_s}{q_s} \ln n \right) ,$$

$$\vec{B} = F \vec{\nabla} \zeta + \vec{\nabla} \psi \times \vec{\nabla} \zeta .$$

Here we have made a number of minor approximations and simplifications of the complete equations.^{3,4} In the electron continuity equation, we have neglected the electron polarization drift, the classical and neoclassical diffusion terms, and the motion of the flux surfaces ($\partial \psi / \partial t \neq 0$). All of these effects are second order in a gyroradius expansion and much smaller than the terms retained in Eq. (1)

for $k_{\perp}\rho_e \ll 1$. In Eqs. (3) and (4), we have neglected the electron viscous stress effects because they are of order $(m_e/m_i)^{1/2} \ll 1$ compared to the ion viscous stress effects that are retained. Finally, we have approximated the toroidal current J_{ζ} by the parallel current J_{\parallel} , which is correct to second order in the small-aspect-ratio expansion $\epsilon \equiv r/R_0 \ll 1$.

The viscous stress terms in Eqs. (1)–(4) may be related to the neoclassically driven pressure anisotropy, given by the Chew-Goldberger-Low form ($\hat{b} \equiv \vec{B}/B$)

$$\vec{\Pi}_{\parallel} = (p_{\parallel} - p_{\perp})(\hat{b}\hat{b} - \vec{I}/3) , \quad (5)$$

where $p_{\parallel} - p_{\perp}$ may be expressed⁴ for species s in terms of the viscous damping frequency μ_s , the magnetic field B , the mass density $n_s m_s$, and the flow velocity \vec{V}_s as

$$p_{\parallel} - p_{\perp} = -\frac{m_s n_s \mu_s \langle B^2 \rangle}{\langle (\hat{b} \cdot \vec{\nabla} B)^2 \rangle} (\vec{V}_s \cdot \vec{\nabla} \ln B) , \quad (6)$$

with

$$\vec{V}_s \cdot \vec{\nabla} \ln B = U_{\theta s} (\hat{b} \cdot \vec{\nabla} B) + V_{rs} \frac{\partial \ln B}{\partial r}$$

and

$$U_{\theta s} = \frac{\vec{V}_s \cdot \vec{\nabla} \theta}{\vec{B} \cdot \vec{\nabla} \theta} = \frac{V_{\parallel s}}{B} + \frac{F}{B^2} \frac{\partial}{\partial \psi} \left(\phi + \frac{T_s}{q_s} \ln n \right) .$$

The divergence of $\vec{\Pi}_{\parallel}$ is then

$$\vec{\nabla} \cdot \vec{\Pi}_{\parallel} = (p_{\parallel} - p_{\perp}) [(\hat{b} \cdot \vec{\nabla}) \hat{b} - \hat{b}(\hat{b} \cdot \vec{\nabla}) \ln B] + \hat{b}(\hat{b} \cdot \vec{\nabla})(p_{\parallel} - p_{\perp}) - \vec{\nabla}(p_{\parallel} - p_{\perp})/3 . \quad (7)$$

From this the parallel viscous stress is

$$\vec{B} \cdot \vec{\nabla} \cdot \vec{\Pi}_{\parallel} = \frac{2}{3} (\vec{B} \cdot \vec{\nabla})(p_{\parallel} - p_{\perp}) - \frac{(p_{\parallel} - p_{\perp})}{B} (\vec{B} \cdot \vec{\nabla}) B . \quad (8)$$

The $\vec{B} \times \vec{\nabla} \cdot \vec{\Pi}_{\parallel}$ viscous stress term of Eq. (3) is then

$$\frac{\vec{B} \times \vec{\nabla} \cdot \vec{\Pi}_{\parallel}}{B^2} = \frac{2}{3} \hat{b} \times \frac{\vec{\nabla}(p_{\parallel} - p_{\perp})}{B} - \frac{(p_{\parallel} - p_{\perp}) J_{\parallel}}{B^2 \mu_0} - \frac{(p_{\parallel} - p_{\perp})}{B^2} \hat{b} \times \vec{\nabla} B . \quad (9)$$

If we assume [see Eq. (6)] that $\beta_{\parallel} - \beta_{\perp} \sim \beta(\rho/l) \ll 1$, then the cross-viscous stress may be approximated as

$$\frac{\vec{B} \times \vec{\nabla} \cdot \vec{\Pi}_{\parallel}}{B^2} \simeq -\frac{(p_{\parallel} - p_{\perp})}{B^2} \hat{b} \times \vec{\nabla} B . \quad (10)$$

We then evaluate the divergence of $(\vec{B} \times \vec{\nabla} \cdot \vec{\Pi}_{\parallel}/B^2)$ assuming low β and retaining terms only to first order in the inverse aspect ratio ($\epsilon \equiv r/R_0 \ll 1$):

$$-\vec{\nabla} \cdot \left[\frac{(p_{\parallel} - p_{\perp}) \hat{b}}{B^2} \times \vec{\nabla} B \right] \simeq -\vec{\nabla} \cdot \left[\frac{(p_{\parallel} - p_{\perp}) \hat{e}_{\zeta}}{B^2} \times \vec{\nabla} B_{\zeta} \right] \quad (11)$$

$$\simeq -\frac{R^2}{2\sqrt{g}} \left[\frac{\partial}{\partial r} \left(\frac{1}{R^2} \right) \frac{\partial}{\partial \theta} - \frac{\partial}{\partial \theta} \left(\frac{1}{R^2} \right) \frac{\partial}{\partial r} \right] \left[\frac{(p_{\parallel} - p_{\perp})}{B^2} \right], \quad (12)$$

where $\sqrt{g} = \vec{\nabla} r \cdot \vec{\nabla} \theta \times \vec{\nabla} \zeta$ is the Jacobian of the transformation to r, θ, ζ coordinates with r being a flux variable.

Equations (8) and (9) for the viscous stresses complete the closure of the moment equations (1)–(4). We express each of the dynamical quantities in Eqs. (1)–(4) as an equilibrium component, f_0 , plus a perturbation, \tilde{f} , and linearize about f_0 . The equilibrium is obtained using the axisymmetric noncircular toroidal code RSTEQ (ref. 11), which solves the Grad-Shafranov equation with $v_{\perp,eq} = V_{\parallel,eq} = \phi_{eq} = 0$. The evolution equations for ψ ($\equiv -RA_{\parallel}$), U ($\equiv \vec{\nabla}_{\perp} \cdot [\rho_0 \vec{\nabla}_{\perp} \phi]$), ρ , and $V_{\parallel i}$ are then given in nondimensional form as

$$\frac{\partial \psi}{\partial t} = \nabla_{\parallel}^{(0)} \phi + \eta J_{\parallel} - \frac{\omega_{*e}}{\rho_0} \nabla_{\parallel} \rho + \frac{\tilde{\mu}_e}{\omega_{cye}} \left(\frac{R^2}{4\epsilon^2 q} \right) \left[\Lambda_e \frac{\partial}{\partial \theta} \left(\frac{1}{R^2} \right) + \frac{4q}{3R^2} \nabla_{\parallel} \Lambda_e \right], \quad (13)$$

$$\begin{aligned} \frac{\partial U}{\partial t} = & S^2 \nabla_{\parallel} J_{\parallel} + \frac{S^2 \beta}{\epsilon} \hat{\zeta} \cdot \vec{\nabla} \rho \times \vec{\kappa} + R_U^{-1} \nabla_{\perp}^2 U \\ & - \frac{\tilde{\mu}_i F \rho_0}{4\epsilon^2 r} \left[\frac{\partial}{\partial \theta} \left(\frac{1}{R^2} \right) \frac{\partial \Lambda_i}{\partial r} - \frac{\partial}{\partial r} \left(\frac{1}{R^2} \right) \frac{1}{r} \frac{\partial \Lambda_i}{\partial \theta} \right], \end{aligned} \quad (14)$$

$$\frac{\partial \rho}{\partial t} = \frac{d\rho_0}{dr} \frac{1}{r} \frac{\partial \phi}{\partial \theta} + D_p \nabla_{\perp}^2 \rho + \frac{2\epsilon^2 S^2 \omega_{*e}}{R^2 \beta_0} \nabla_{\parallel} J_{\parallel} - \frac{\epsilon \rho_0}{R^2} \nabla_{\parallel}^{(0)} (RV_{\parallel i}), \quad (15)$$

$$\frac{\partial (RV_{\parallel i})}{\partial t} = -\frac{S^2 \beta_0 R^2 T_e}{2\epsilon \rho_0} \nabla_{\parallel} \rho + \frac{\tilde{\mu}_i R^2}{4\epsilon q} \left[\Lambda_i \frac{\partial}{\partial \theta} \left(\frac{1}{R^2} \right) + \frac{4}{3} \frac{q}{R^2} \nabla_{\parallel} \Lambda_i \right], \quad (16)$$

where $\omega_{*e} = \omega_{diamag,e} \tau_R = (\beta_0 S^2 / 2\epsilon^2 \omega_{cye})$, $\tilde{\mu}_{i,e} = \tau_R \mu_{i,e}$, $\tau_R = \mu_0 a^2 / \eta_0$, $\tau_{Hp} = R_0 / v_A$, $\omega_{cye} = \Omega_{ci} \tau_R$, $\omega_{cye} = \Omega_{ce} \tau_R$, $S = \tau_R / \tau_{Hp}$, $\beta_0 = 2\mu_0 p_0 / B_{\zeta 0}^2$,

$$\nabla_{\parallel}^{(0)} \chi = R_0 R(\hat{b}_0 \cdot \vec{\nabla} \chi) = \frac{\partial \chi^{(1)}}{\partial \zeta} - \frac{1}{q} \frac{\partial \chi^{(1)}}{\partial \theta},$$

with $\chi =$ one of the dynamical variables,

$$\nabla_{\parallel} \chi = R_0 R(\hat{b} \cdot \vec{\nabla} \chi) = \nabla_{\parallel}^{(0)} \chi^{(1)} + \left(\frac{1}{r} \right) \left[\frac{\partial \psi}{\partial r} \frac{\partial \chi^{(0)}}{\partial \theta} - \frac{\partial \psi}{\partial \theta} \frac{\partial \chi^{(0)}}{\partial r} \right],$$

$$\Lambda_{i,e} = K_0(r) \left\{ -\frac{\epsilon}{q} \frac{\partial}{\partial \theta} \left(\frac{1}{R^2} \right) RV_{\parallel i,e} + \frac{R^2}{rF'} \left[\frac{\partial}{\partial \theta} \left(\frac{1}{R^2} \right) \frac{\partial \phi_{*i,e}}{\partial r} - \frac{\partial}{\partial r} \left(\frac{1}{R^2} \right) \frac{\partial \phi_{*i,e}}{\partial \theta} \right] \right\} ,$$

with $\phi_{*e} = \phi - \omega_{*e} \ln \rho$ and $\phi_{*i} = \phi + \omega_{*i} \ln \rho$ (we take $\omega_{*i} = 0$ here),

$$RV_{\parallel e} = RV_{\parallel i} - \left(\frac{S^2}{\epsilon \omega_{cyi}} \right) \frac{J_{\parallel}}{\rho_0} , \quad J_{\parallel} = \hat{b} \cdot \vec{J} ,$$

$$K_0(r) = \frac{4q^2 \langle 1/R^2 \rangle}{\langle [\partial/\partial \theta (1/R^2)]^2 \rangle} = \frac{\langle B^2 \rangle}{R_0^2 \langle (\hat{b} \cdot \vec{\nabla} B)^2 \rangle} .$$

The D_p term in Eq. (15) is an artificial diffusion term inserted to assist numerical convergence. It can represent classical diffusion if $D_p \sim \beta$ and neoclassical diffusion if $D_p \sim \beta(\mu_e/\nu_e)q^2/\epsilon^2 \lesssim \sqrt{\epsilon}\beta_p$.

The electron and ion neoclassical viscosities¹² are given by

$$\mu_e = \frac{2.3\sqrt{\epsilon}\nu_e}{(1 + 1.07\nu_{*e}^{1/2} + 1.02\nu_{*e})(1 + 1.07\nu_{*e}\epsilon^{3/2})} , \quad (17)$$

$$\mu_i = \frac{0.66\sqrt{\epsilon}\nu_i}{(1 + 1.03\nu_{*i}^{1/2} + 0.31\nu_{*i})(1 + 0.66\nu_{*i}\epsilon^{3/2})} , \quad (18)$$

where $\nu_* \equiv \nu\epsilon^{-3/2}R_0q/v_{th}$ and $\epsilon \equiv r/R_0$ is the local aspect ratio.

Here all times are normalized to the resistive diffusion time $\tau_R = \mu_0 a^2/\eta_0$, a is a generalized minor radius, R is the major radius divided by R_0 (the major radius of the magnetic axis), and ∇_{\parallel} is normalized by R_0 , ∇_{\perp} is normalized by a , the resistivity is normalized to η_0 (its value at the magnetic axis), the magnetic fields to $B_{\zeta 0}$ (the vacuum field at R_0), \vec{v}_{\perp} to a/τ_R , J_{\parallel} to $B_{\zeta 0}/\mu_0 R_0$, ϕ to $a^2 B_{\zeta 0}/\tau_R$, ψ to $a^2 B_{\zeta 0}$, and the curvature $\vec{\kappa}$ normalized to R_0 . These equations are solved on a generalized nonorthogonal coordinate system (r, θ, ζ) (ref. 13) determined by the equilibrium code. The generalized radial variable r is an equilibrium flux surface label, $0 \leq r \leq 1$, θ is a generalized poloidal angle variable, and ζ is the usual geometric toroidal angle.

III. NUMERICAL RESULTS

The goals in solving Eqs. (13)–(16) numerically were (a) to examine the transition from a resistive ballooning mode to a neoclassical pressure-gradient-driven instability by gradually increasing the neoclassical viscosity, (b) to check the scaling of the neoclassical instability with respect to the relevant physical parameters and compare it with analytic predictions, and (c) to test the effects of the presence

and absence of various terms, such as the sound wave coupling (parallel compressibility), parallel ion flow evolution, resistivity, and classical viscosity.

The code used in solving Eqs. (13)–(16) is an extension of the FAR code.¹⁰ This code employs a finite difference representation in the radial coordinate r and a Fourier series expansion in the poloidal and toroidal angles θ and ζ . The resulting matrix equations are then evolved in time using a fully implicit technique. Perturbed quantities are represented in the following form, which allows for general symmetries:

$$f(r, \theta, \zeta) = \sum f_l(r) \cos(m\theta + n\zeta) + \sum f_{l-}(r) \sin(m\theta + n\zeta) . \quad (19)$$

This form is necessary because the neoclassical terms included in Eqs. (13)–(16) do not conserve the normal symmetries present in the reduced resistive MHD equations [i.e., ϕ and $V_{\parallel i}$ would normally involve only $\sin(m\theta + n\zeta)$ components, while ψ and ρ would involve only $\cos(m\theta + n\zeta)$ components]. This fact also implies that the eigenvalue will have a real frequency as well as a growth rate. Normally, 11 poloidal modes at a fixed toroidal mode number are included in each summation with the spectrum centered on $m = 6$ – 9 , depending on the parameter regime being studied.

The numerical results presented here are based upon a slightly simplified version of Eqs. (13)–(16). First, the $\nabla_{\parallel} \Lambda_{e,i}$ terms in Eqs. (13) and (16) have been neglected. The remaining neoclassical term in Eq. (13) has then been flux surface averaged. Preliminary calculations carried out without invoking these approximations indicate no significant qualitative changes from the results presented here. Also, we do not retain the ω_{*e} terms here, except as they enter into ϕ_{*e} , and, as mentioned previously, ω_{*i} is neglected.

Parameters that remain fixed through most of the following results are $S = 10^5$, $\omega_{cyi} = 3 \times 10^6$, $\epsilon = 0.25$, central plasma beta $\beta_0 = 0.087$ (except where β_0 scaling is examined), and toroidal mode number $n = 6$ (except where n scaling is examined). This value of n is expected to be large enough for the parameters considered here to reasonably allow comparison with the asymptotic ($n \rightarrow \infty$) ballooning mode analytic theory of neoclassical MHD pressure-gradient-driven instabilities.^{2,4,6,7}

We first study the transition from a resistive ballooning instability to a neoclassical MHD instability. In Fig. 1 the growth rate is plotted as a function of the neoclassical electron viscosity parameter μ_e/ν_e . Here we have left out the $\nabla_{\parallel}(RV_{\parallel i})$ term in the density evolution equation (15). This term introduces parallel compressibility and would strongly stabilize the resistive ballooning mode (the effect

of this is discussed later). As indicated, the expected breakpoint between the resistive Pfirsch-Schlüter and neoclassical plateau regimes occurs around $\mu_e/\nu_e = \epsilon^2$. The growth rate in the resistive regime ($\mu_e/\nu_e < \epsilon^2$) drops slightly with increasing μ_e/ν_e but remains close to its pure resistive ($\mu_e/\nu_e = 0$) value. In the vicinity of $\mu_e/\nu_e = \epsilon^2$ the growth rate begins to take on a different scaling with respect to μ_e/ν_e , the slope of which approaches that of the analytic prediction,^{2,4,6,7}

$$\gamma = \frac{n^{2/3} q^{2/3}}{\tau_{H\theta} S_\theta^{1/3}} \left(\frac{\mu_e}{\nu_e} \right)^{1/3} \left(\frac{\beta_\theta}{2r_p} \right)^{2/3}, \quad (20)$$

where $\beta_\theta = 8\pi p/B_\theta^2$, $r_p^{-1} = r|d\ln p/dr|$, $S_\theta = \tau_R/\tau_{A\theta}$, $\tau_{A\theta} = (4\pi\rho_m)^{1/2} R_0 q/B_\theta$. The dotted line of Fig. 1 shows Eq. (20) evaluated locally in radius near the peaking of the mode structure of the numerical results. The two results are about a factor of two different in magnitude, but the slopes are very similar. This difference in magnitude can largely be accounted for by the fact that the analytic theory does not include the $\hat{b} \cdot \vec{\nabla} p \times \vec{\kappa}$ term in the vorticity equation (14) that drives the conventional resistive ballooning instability. In the numerical results, we retained this term because we wanted to carefully follow the transition from resistive ballooning to the neoclassical pressure-gradient-driven instability, and the term was needed for the existence of the resistive mode.

Figure 2 indicates that closer agreement in magnitude is obtained with the analytic prediction when the pressure gradient curvature term in Eq. (14) is absent (dashed line). The small remaining discrepancy between the dashed and dotted lines (analytic prediction) can be attributed to several differences between the analytic and numerical models. First, the analytic theory is local to a flux surface, while the eigenfunctions in the numerical results have a distributed radial mode structure. Also, the numerical results are based upon a relatively finite value of toroidal mode number ($n = 6$), while the analysis is asymptotic in n ($n \rightarrow \infty$). A final difference is that the radial flow terms ($\propto V_r$) in Eq. (6) had to be included in the code to maintain regularity at the origin, whereas these terms were neglected in the analysis. The other significant aspect of Fig. 2 is its demonstration of the fact that the drive for the neoclassical pressure-gradient-driven instability comes from a source (the fluctuating bootstrap current) other than the usual pressure gradient curvature term that drives resistive ballooning instabilities.

Besides the altered growth rate, a further distinguishing characteristic of the neoclassical pressure-gradient-driven instability is a modification in the mode structure. As μ_e/ν_e is increased, the mode is expected to broaden radially from the highly

peaked structure of the resistive ballooning instability.^{2,4,6} This feature is demonstrated in Fig. 3, which displays contour plots of the perturbed potential function and the radial mode structure of the dominant poloidal mode of the potential for several of the cases of Fig. 1. As μ_e/ν_e is increased into the neoclassical regime ($\mu_e/\nu_e \geq \epsilon^2 = 0.0625$), the radial mode structure broadens and assumes a roughly Gaussian shape, in contrast to the highly peaked resistive ballooning mode limit ($\mu_e/\nu_e = 0$). Also, the dominant poloidal mode number shifts upward slightly, and the peak in the potential moves outward in radius with increasing μ_e/ν_e . This effect is probably caused by the radial dependence ($\propto r^2$) of the neoclassical viscosities used in the code. Analytic predictions of the radial width scaling of the neoclassical pressure-gradient-driven instability^{2,4,6} result in

$$\delta_\mu = \frac{r}{(2qr_q)^{1/2} n^{1/3} S_\theta^{1/3}} \left[\left(\frac{\mu_e}{\nu_e} \right)^2 \left(\frac{\beta_\theta}{2r_p} \right) \right]^{1/6}. \quad (21)$$

Local evaluations of δ_μ near the peak in the numerical radial mode structure are shown in Fig. 4, along with the measured width at half-maximum of the dominant poloidal potential mode in the numerical results. These evaluations are for cases shown in Fig. 1. Again, the slopes with respect to μ_e/ν_e are similar, but the magnitudes differ for reasons similar to those given for the discrepancies in magnitude of the growth rates in Fig. 1.

It is also of interest to check the scaling with respect to two other parameters, β and n (toroidal mode number), that occur in Eq. (20). The numerical results and local evaluations of Eq. (20) are compared in Figs. 5 and 6. The slopes indicate good agreement with the $\beta^{2/3}$ and $n^{2/3}$ scalings. The analytic predictions deviate from straight lines here as a result of the radial and poloidal mode number shifts that occur in the dominant mode in the numerical results as β_0 and n are varied.

Parallel compressibility has been found to be a strongly stabilizing mechanism for resistive ballooning instabilities.⁹ As mentioned earlier, the results presented so far have neglected parallel compressibility, which can be included in our equations through the $\nabla_{\parallel}(RV_{\parallel i})$ term in the density evolution equation (15). Figure 7 presents a comparison of the results given in Fig. 1 with (dashed line) and without (solid line) compressibility. As expected, parallel compressibility is strongly stabilizing in the resistive regime ($\mu_e/\nu_e < 0.06$). In the neoclassical regime ($\mu_e/\nu_e > 0.06$), compressibility is still stabilizing, but to a much lesser extent than for the resistive ballooning mode.

The neoclassical MHD evolution equations presented here incorporate the proper damping of the poloidal ion flow velocity. This damping is caused by collisions between trapped and untrapped particles in the plateau and banana regimes and by magnetic compression/expansion from the θ dependence of the magnetic field in the Pfirsch-Schlüter regime. An approximation commonly used in the analysis^{2,4,6} is that the ion parallel flow is rapidly damped so that the neoclassical term in the $V_{\parallel i}$ equation (16) can be set equal to zero, resulting in $V_{\parallel i} \simeq (q/r\epsilon F)(\partial\phi/\partial r)$. This approximation is checked in Fig. 8, where the growth rate vs μ_e/ν_e is plotted both with the full $V_{\parallel i}$ equation time evolved (solid line) and with the rapid damping limit (dashed line) and compressibility absent. This indicates that, for the parameters considered here, this is a fairly good approximation, as would be expected since the parallel ion flow damping time is fast compared to the growth of the instability.

One further effect of interest for the neoclassical pressure-gradient-driven instability is that of resistivity. In Fig. 9, growth rates both with (solid line) and without (dashed line) resistivity are plotted vs μ_e/ν_e with compressibility present. In the neoclassical regime, resistivity seems to have only a very weak influence because of the dominant effect of the dissipation from the neoclassical viscous damping.

Another form of classical dissipation that could influence the neoclassical pressure-gradient-driven instability is the classical viscous damping term in the vorticity equation (14) (i.e., the $R_U^{-1}\nabla_{\perp}^2 U$ term). This term has not been present in the results given so far. Its effect is considered in Fig. 10 for one of the ideal cases shown in Fig. 9. The classical viscosity may be expressed in terms of other physical parameters as $R_U^{-1}\tau_{Hp} = S^{-1}\Omega_{ci}\tau_R(\rho_i/a)^2$, where Ω_{ci} is the ion cyclotron frequency and ρ_i is the ion gyroradius; a typical value of $R_U^{-1}\tau_{Hp}$ for the parameters used here is $\simeq 8 \times 10^{-3}$. These results indicate only a slight degree of stabilization at this level. Examination of the radial mode structure indicates some radial broadening as R_U^{-1} is increased, thus yielding a smaller value of $\nabla_{\perp}^2 U$ in the vorticity equation than would be expected with a fixed radial mode structure.

IV. CONCLUSIONS AND SUMMARY

A new form of pressure-gradient-driven instability, which is an extension of the resistive ballooning mode into high-temperature regimes, has been analyzed numerically. This instability arises from including the appropriate modifications to the plasma flows and currents caused by neoclassical MHD effects. The instability

examined here is driven primarily through the fluctuating bootstrap current in Ohm's law. It has higher growth rates than the resistive ballooning instability and a broadened radial mode structure in the neoclassical regime.

We have used a 3-D toroidal initial-value code that includes the relevant neoclassical MHD corrections to resistive MHD. In the appropriate limits, this code has reproduced the analytically expected scalings for the growth rate of the instability with respect to the neoclassical viscosity parameter μ_e/ν_e , the toroidal mode number n , and the plasma beta. Since the code includes the driving terms for both the new neoclassical instability and the resistive ballooning mode, it provides a means of carefully examining the transition from one type of instability to the other. In addition, the influence of several new effects such as compressibility stabilization, classical viscosity, resistivity, and self-consistent ion parallel flow evolution can be easily checked. The main conclusion is that the neoclassical pressure-gradient-driven instability seems to be resilient against many of the mechanisms, such as parallel compressibility, that tend to be strongly stabilizing for the resistive ballooning mode. This could be of importance in understanding confinement in higher-temperature plasmas operating in the long mean-free-path regime.

REFERENCES

- ¹S. P. Hirshman and D. J. Sigmar, Nucl. Fusion **21**, 1079 (1981).
- ²J. D. Callen and K. C. Shaing, Phys. Fluids **28**, 1845 (1985).
- ³J. D. Callen and K. C. Shaing, see National Technical Information Service Document No. DE-86009463/XAB University of Wisconsin Technical Report UWPR 85-8). Copies may be ordered from the National Technical Information Service, Springfield, Virginia 22161. The price is \$11.95 plus a \$3.00 handling fee. All orders must be prepaid.
- ⁴J. D. Callen, W. X. Qu, K. D. Siebert, B. A. Carreras, K. C. Shaing, and D. A. Spong, in *Proceedings of the 11th International Conference on Plasma Physics and Controlled Nuclear Fusion Research (Kyoto, Japan, November 13-20, 1986)* (International Atomic Energy Agency, Vienna, 1987), Vol. 2, p. 157.
- ⁵M. Kotschenreuther, A. Aydemir, R. Carrera, R. D. Hazeltine, J. D. Meiss, and P. J. Morrison, in *Proceedings of the 11th International Conference on Plasma Physics and Controlled Nuclear Fusion Research (Kyoto, Japan, November 13-20, 1986)* (International Atomic Energy Agency, Vienna, 1987), Vol. 2, p. 149.
- ⁶K. C. Shaing and J. D. Callen, Phys. Fluids **28**, 1859 (1985).
- ⁷J. W. Connor and L. Chen, Phys. Fluids **28**, 2201 (1985).
- ⁸B. A. Carreras, P. H. Diamond, M. Murakami, J. L. Dunlap, J. D. Bell, H. R. Hicks, J. A. Holmes, C. E. Thomas, and R. M. Wieland, Phys. Rev. Lett. **50**, 503 (1983).
- ⁹T. C. Hender, B. A. Carreras, W. A. Cooper, J. A. Holmes, P. H. Diamond, and P. L. Similon, Phys. Fluids **27**, 1439 (1984).
- ¹⁰L. A. Charlton, J. A. Holmes, H. R. Hicks, V. E. Lynch, and B. A. Carreras, J. Comput. Phys. **63**, 107, (1986).
- ¹¹J. A. Holmes, Y-K. M. Peng, and S. J. Lynch, J. Comput. Phys. **36**, 35 (1980).
- ¹²F. L. Hinton and R. D. Hazeltine, Rev. Mod. Phys. **48**, 239 (1976).
- ¹³B. A. Carreras, H. R. Hicks, and D. K. Lee, Phys. Fluids **24**, 66 (1981).

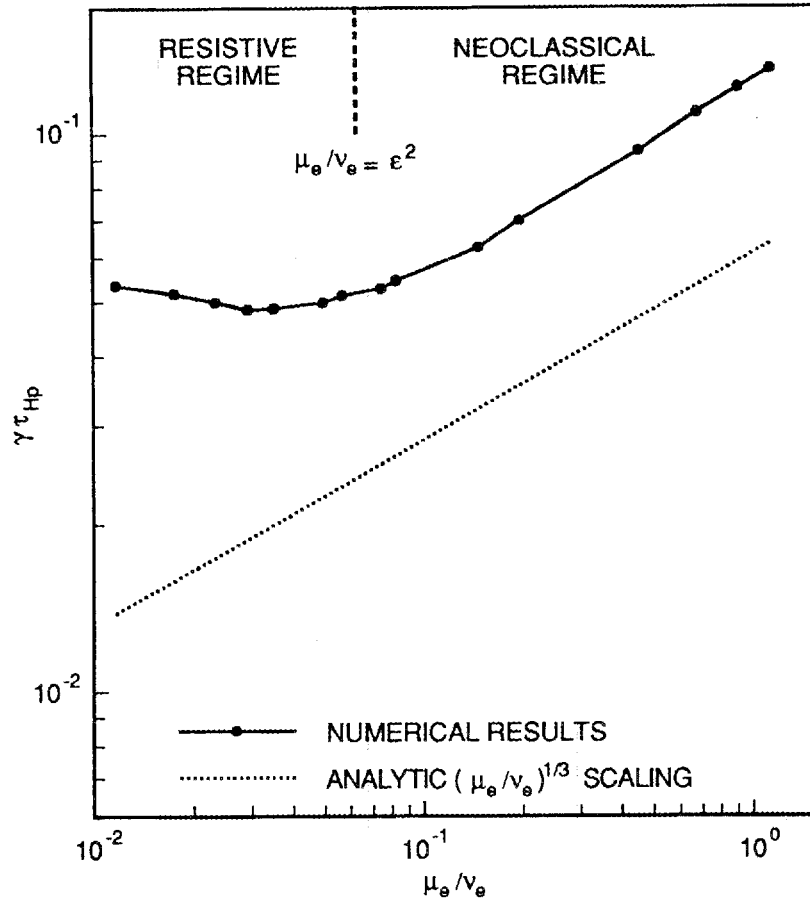


Fig. 1. Growth rate vs electron neoclassical viscosity parameter μ_e / ν_e in resistive and neoclassical regimes from numerical results (solid line) and analytic scaling (dotted line) ($n = 6$, $\beta_0 = 0.087$, $S = 10^5$, $\omega_{cyl} = 3 \times 10^6$, incompressible).

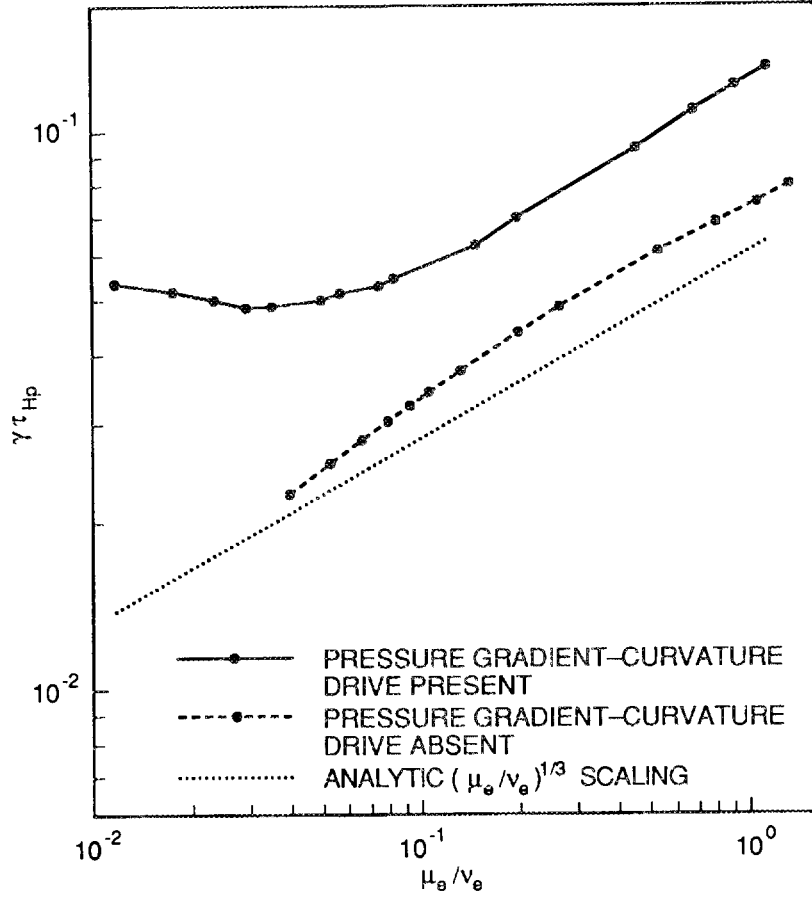


Fig. 2. Growth rate vs electron neoclassical viscosity parameter μ_e/ν_e in resistive and neoclassical regimes with (solid line) and without (dashed line) pressure gradient curvature drive in vorticity equation ($n = 6$, $\beta_0 = 0.087$, $S = 10^5$, $\omega_{cyi} = 3 \times 10^6$, incompressible).

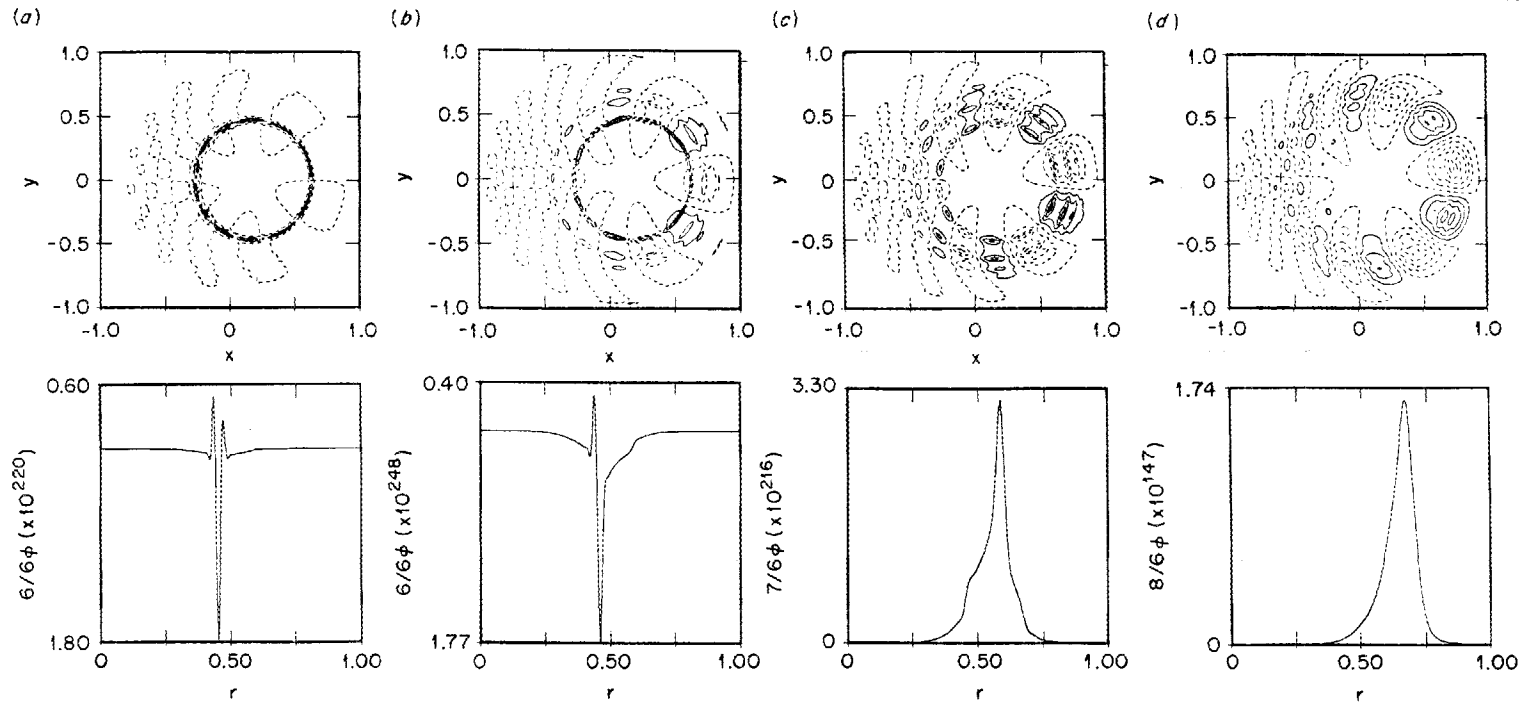


Fig. 3. Perturbed potential contour plots and radial dependence of dominant poloidal mode for parameters of Fig. 1 with (a) $\mu_e/\nu_e = 0$, (b) $\mu_e/\nu_e = 0.03$, (c) $\mu_e/\nu_e = 0.05$, and (d) $\mu_e/\nu_e = 0.22$.

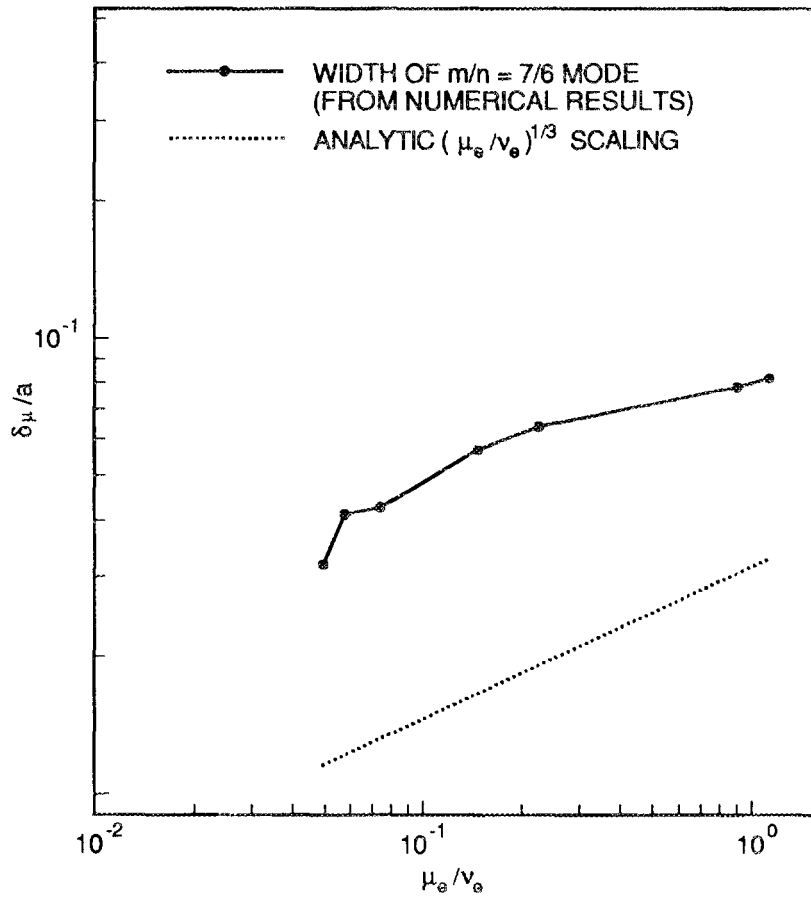


Fig. 4. Scalings of radial mode width vs μ_e/ν_e from numerical (solid line) and analytical (dotted line) calculations based on the results given in Fig. 1.

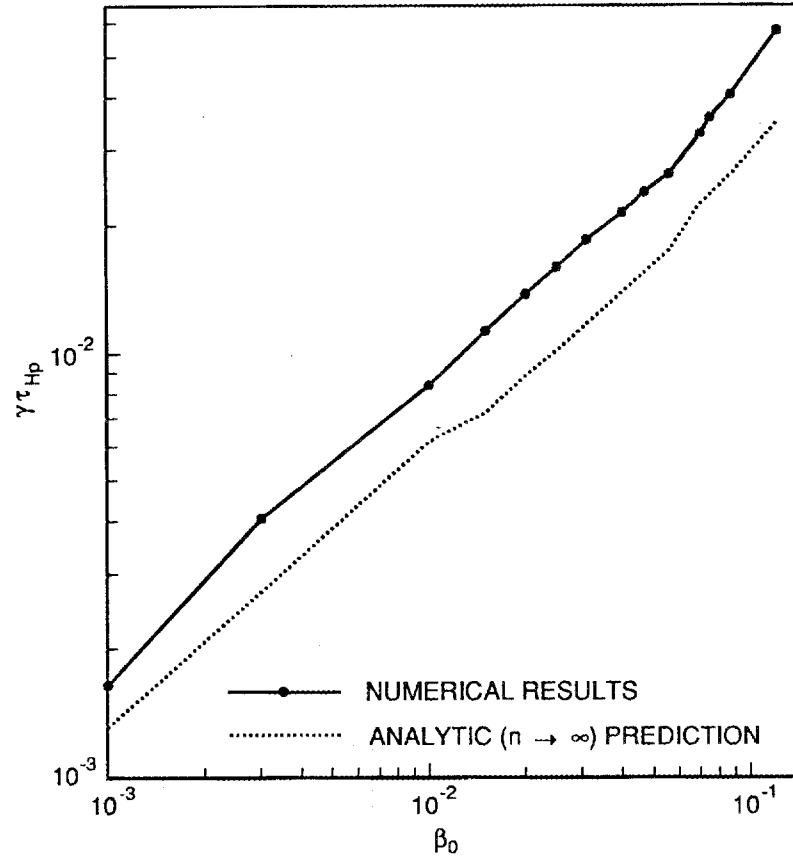


Fig. 5. Numerical (solid line) and analytical (dotted line) scalings of growth rate vs β_0 , peak plasma beta ($n = 6$, $\beta_0 = 0.087$, $S = 10^5$, $\omega_{c yi} = 3 \times 10^6$, incompressible).

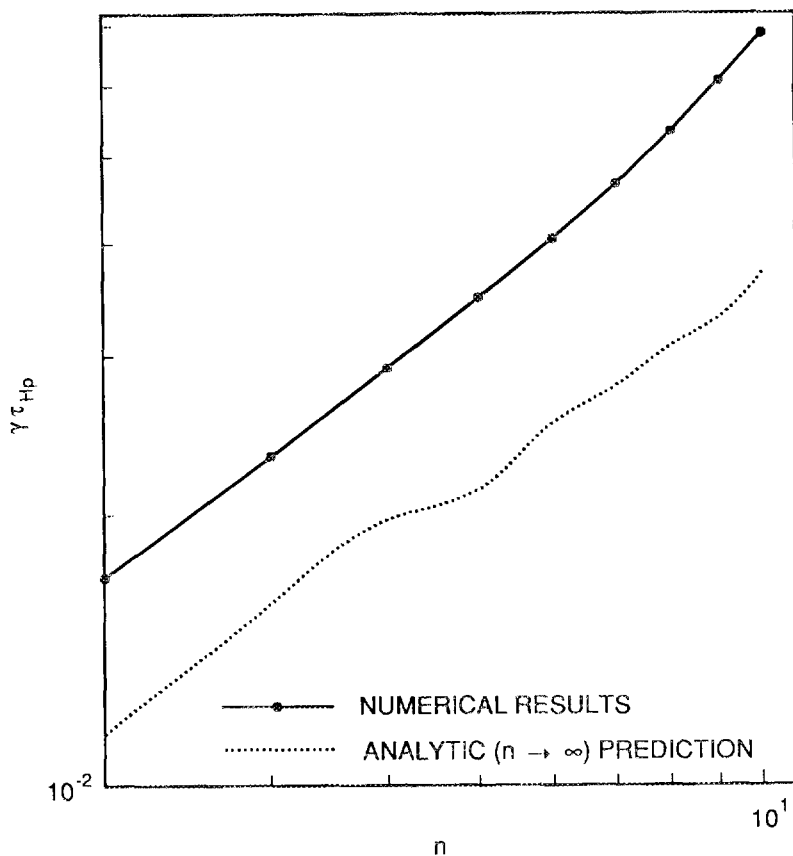


Fig. 6. Numerical (solid line) and analytical (dotted line) scalings of growth rate vs n , toroidal mode number ($n = 6$, $\beta_0 = 0.087$, $S = 10^5$, $\omega_{cyi} = 3 \times 10^6$, incompressible).

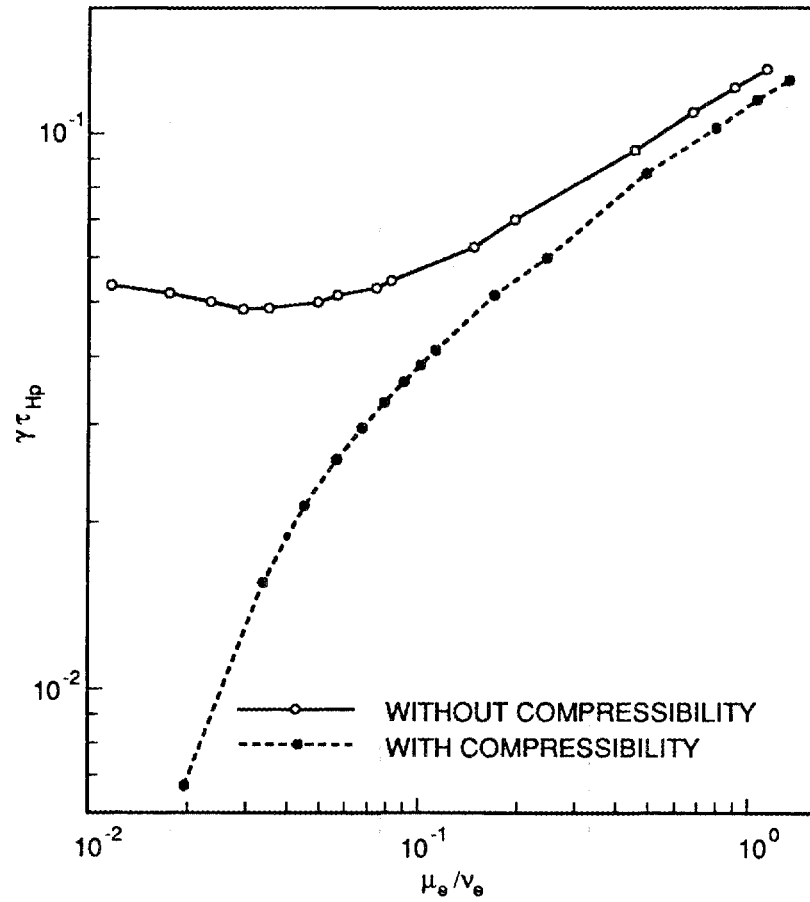


Fig. 7. Scaling of growth rate in resistive and neoclassical regimes with respect to μ_e/ν_e with (dashed line) and without (solid line) parallel compressibility coupling ($n = 6$, $\beta_0 = 0.087$, $S = 10^5$, $\omega_{cyl} = 3 \times 10^6$).

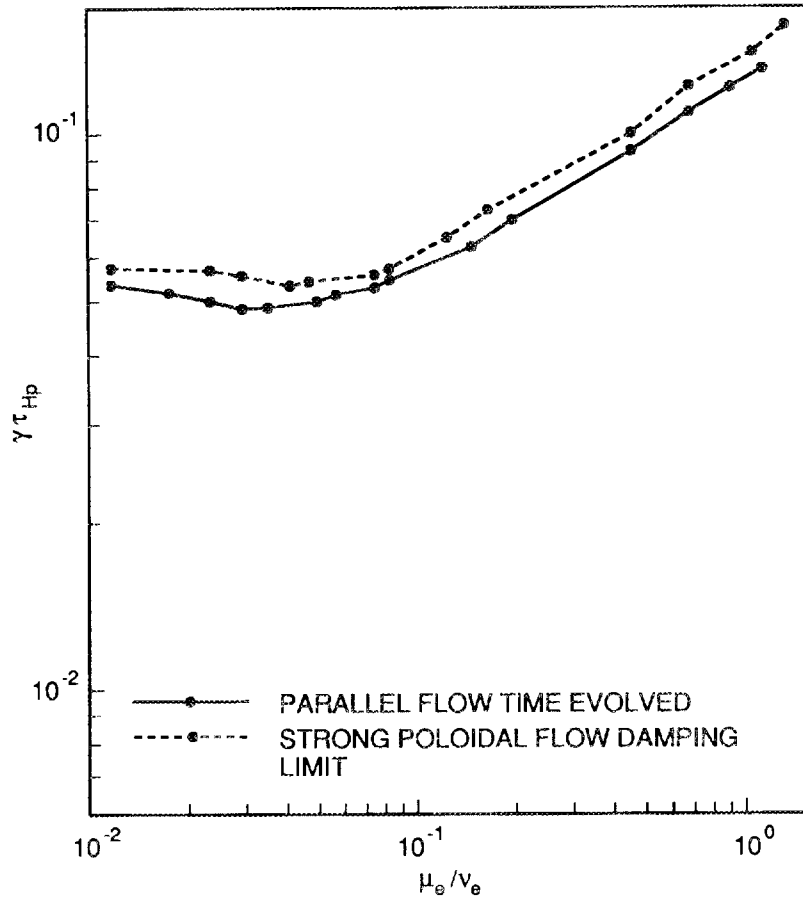


Fig. 8. Scaling of growth rate with respect to μ_e / ν_e with parallel flow equation time evolved (solid line) and under strong poloidal flow damping approximation (dashed line) ($n = 6$, $\beta_0 = 0.087$, $S = 10^5$, $\omega_{cyl} = 3 \times 10^6$, incompressible).

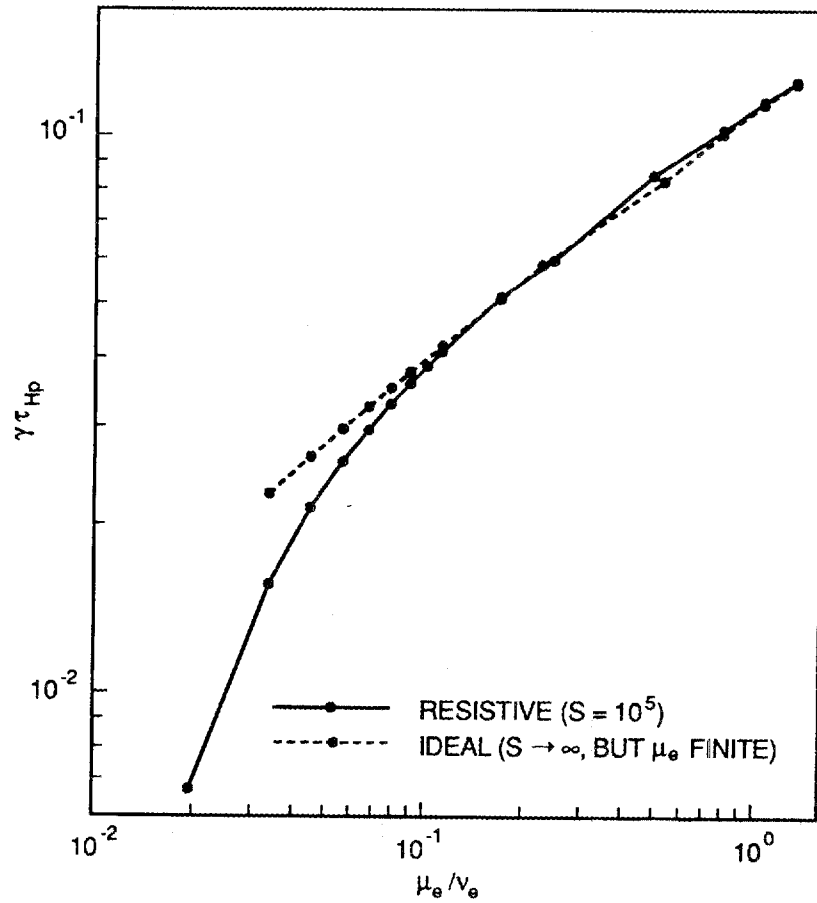


Fig. 9. Scaling of growth rate with respect to μ_e / ν_e with (solid line, $S = 10^5$) and without (dashed line) resistivity ($n = 6$, $\beta_0 = 0.087$, $\omega_{cyl} = 3 \times 10^6$, compressible).

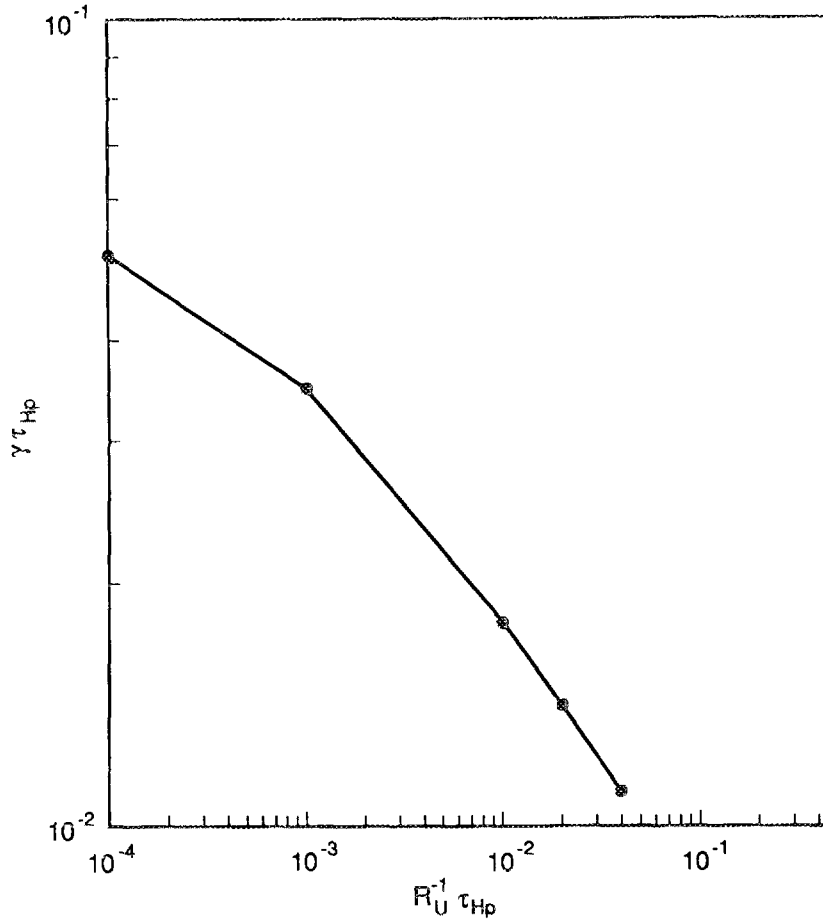


Fig. 10. Dependence of growth rate for a neoclassical pressure-gradient-driven instability on the classical viscosity ($\mu_e/\nu_e = 0.22$, $n = 6$, $\beta_0 = 0.087$, $\omega_{c yi} = 3 \times 10^6$, compressible, ideal case as in Fig. 9).

INTERNAL DISTRIBUTION

- | | | | |
|------|----------------|--------|---|
| 1. | L. A. Berry | 15-16. | K. C. Shaing |
| 2-3. | B. A. Carreras | 17. | J. Sheffield |
| 4-5. | L. A. Charlton | 18-22. | D. A. Spong |
| 6. | N. Dominguez | 23-24. | Laboratory Records Department |
| 7. | C. L. Hedrick | 25. | Laboratory Records, ORNL-RC |
| 8. | R. A. Dory | 26. | Central Research Library |
| 9. | S. P. Hirshman | 27. | Document Reference Section |
| 10. | J. A. Holmes | 28. | Fusion Energy Division Library |
| 11. | W. A. Houlberg | 29-30. | Fusion Energy Division
Publications Office |
| 12. | G. S. Lee | 31. | ORNL Patent Office |
| 13. | J-N. LeBoeuf | | |
| 14. | V. E. Lynch | | |

EXTERNAL DISTRIBUTION

32. Office of the Assistant Manager for Energy Research and Development, U.S. Department of Energy, Oak Ridge Operations Office, P.O. Box E, Oak Ridge, TN 37831
- 33-34. J. D. Callen, Department of Nuclear Engineering, University of Wisconsin, Madison, WI 53706-1687
35. J. F. Clarke, Director, Office of Fusion Energy, Office of Energy Research, ER-50 Germantown, U.S. Department of Energy, Washington, DC 20545
36. R. W. Conn, Department of Chemical, Nuclear, and Thermal Engineering, University of California, Los Angeles, CA 90024
37. S. O. Dean, Fusion Power Associates, Inc., 2 Professional Drive, Suite 248, Gaithersburg, MD 20879
38. H. K. Forsen, Bechtel Group, Inc., Research Engineering, P. O. Box 3965, San Francisco, CA 94119
39. J. R. Gilleland, L-644, Lawrence Livermore National Laboratory, P.O. Box 5511, Livermore, CA 94550
40. R. W. Gould, Department of Applied Physics, California Institute of Technology, Pasadena, CA 91125
41. R. A. Gross, Plasma Research Laboratory, Columbia University, New York, NY 10027
42. D. M. Meade, Princeton Plasma Physics Laboratory, P.O. Box 451, Princeton, NJ 08543

43. M. Roberts, International Programs, Office of Fusion Energy, Office of Energy Research, ER-52 Germantown, U.S. Department of Energy, Washington, DC 20545
44. W. M. Stacey, School of Nuclear Engineering and Health Physics, Georgia Institute of Technology, Atlanta, GA 30332
45. D. Steiner, Nuclear Engineering Department, NES Building, Tibbetts Avenue, Rensselaer Polytechnic Institute, Troy, NY 12181
46. R. Varma, Physical Research Laboratory, Navrangpura, Ahmedabad 380009, India
47. Bibliothek, Max-Planck Institut für Plasmaphysik, Boltzmannstrasse 2, D-8046 Garching, Federal Republic of Germany
48. Bibliothek, Institut für Plasmaphysik, KFA Jülich GmbH, Postfach 1913, D-5170 Jülich, Federal Republic of Germany
49. Bibliothek, KfK Karlsruhe GmbH, Postfach 3640, D-7500 Karlsruhe 1, Federal Republic of Germany
50. Bibliothéque, Centre de Recherches en Physique des Plasmas, Ecole Polytechnique Fédérale de Lausanne, 21 Avenue des Bains, CH-1007 Lausanne, Switzerland
51. R. Aymar, CEN/Cadarache, Departement de Recherches sur la Fusion Contrôlée, F-13108 Saint-Paul-lez-Durance Cedex, France
52. Bibliothèque, CEN/Cadarache, F-13108 Saint-Paul-lez-Durance Cedex, France
53. Library, Culham Laboratory, UKAEA, Abingdon, Oxfordshire, OX14 3DB, England
54. Library, JET Joint Undertaking, Abingdon, Oxfordshire OX14 3EA, England
55. Library, FOM-Instituut voor Plasmafysica, Rijnhuizen, Edisonbaan 14, 3439 MN Nieuwegein, The Netherlands
56. Library, Institute of Plasma Physics, Nagoya University, Chikusa-ku, Nagoya 464, Japan
57. Library, International Centre for Theoretical Physics, P.O. Box 586, I-34100 Trieste, Italy
58. Library, Centro Recherche Energia Frascati, C.P. 65, I-00044 Frascati (Roma), Italy
59. Library, Plasma Physics Laboratory, Kyoto University, Gokasho, Uji, Kyoto 611, Japan
60. Plasma Research Laboratory, Australian National University, P.O. Box 4, Canberra, A.C.T. 2601, Australia
61. Library, Japan Atomic Energy Research Institute, Naka Fusion Research Establishment, 801-1 Mukoyama, Naka-machi, Naka-gun, Ibaraki-ken, Japan
62. G. A. Eliseev, I. V. Kurchatov Institute of Atomic Energy, P. O. Box 3402, 123182 Moscow, U.S.S.R.

63. V. A. Glukhikh, Scientific-Research Institute of Electro-Physical Apparatus, 188631 Leningrad, U.S.S.R.
64. I. Shpigel, Institute of General Physics, U.S.S.R. Academy of Sciences, Ulitsa Vavilova 38, Moscow, U.S.S.R.
65. D. D. Ryutov, Institute of Nuclear Physics, Siberian Branch of the Academy of Sciences of the U.S.S.R., Sovetskaya St. 5, 630090 Novosibirsk, U.S.S.R.
66. V. T. Tolok, Kharkov Physical-Technical Institute, Academical St. 1, 310108 Kharkov, U.S.S.R.
67. Deputy Director, Southwestern Institute of Physics, P.O. Box 15, Leshan, Sichuan, China (PRC)
68. Director, The Institute of Plasma Physics, P.O. Box 26, Hefei, Anhui, China (PRC)
69. D. Crandall, Experimental Plasma Research Branch, Division of Development and Technology, Office of Fusion Energy, Office of Energy Research, ER-542 Germantown, U.S. Department of Energy, Washington, DC 20545
70. N. A. Davies, Office of the Associate Director, Office of Fusion Energy, Office of Energy Research, ER-51 Germantown, U.S. Department of Energy, Washington, DC 20545
71. R. H. McKnight, Experimental Plasma Research Branch, Division of Development and Technology, Office of Fusion Energy, Office of Energy Research, ER-542 Germantown, U.S. Department of Energy, Washington, DC 20545
72. D. B. Nelson, Director, Division of Applied Plasma Physics, Office of Fusion Energy, Office of Energy Research, ER-54 Germantown, U.S. Department of Energy, Washington, DC 20545
73. E. Oktay, Division of Confinement Systems, Office of Fusion Energy, Office of Energy Research, ER-55 Germantown, U.S. Department of Energy, Washington, DC 20545
74. W. Sadowski, Fusion Theory and Computer Services Branch, Division of Applied Plasma Physics, Office of Fusion Energy, Office of Energy Research, ER-541 Germantown, U.S. Department of Energy, Washington, DC 20545
75. R. E. Mickens, Atlanta University, Department of Physics, Atlanta, GA 30314
76. M. N. Rosenbluth, University of California-San Diego, La Jolla, CA 92093-0319
77. Duk-In Choi, Department of Physics, Korea Advanced Institute of Science and Technology, P.O. Box 150, Chong Ryang-Ri, Seoul, Korea
78. Library of Physics Department, University of Ioannina, Ioannina, Greece
79. C. De Palo, Library, Associazione EURATOM-ENEA sulla Fusione, CP 65, I-00044 Frascati (Roma), Italy

80. Theory Department Read File, c/o D. W. Ross, University of Texas, Institute for Fusion Studies, Austin, TX 78712
81. Theory Department Read File, c/o R. Parker, Director, Plasma Fusion Center, NW 16-202, Massachusetts Institute of Technology, Cambridge, MA 02139
82. Theory Department Read File, c/o R. White, Princeton Plasma Physics Laboratory, P.O. Box 451, Princeton, NJ 08543
83. Theory Department Read File, c/o L. Kovrizhnykh, Lebedev Institute of Physics, Academy of Sciences, 53 Leninsky Prospect, 117924 Moscow, U.S.S.R.
84. Theory Department Read File, c/o B. B. Kadomtsev, I. V. Kurchatov Institute of Atomic Energy, P.O. Box 3402, 123182 Moscow, U.S.S.R.
85. Theory Department Read File, c/o T. Kamimura, Institute of Plasma Physics, Nagoya University, Nagoya 464, Japan
86. Theory Department Read File, c/o C. Mercier, Departement de Recherches sur la Fusion Controlee, B.P. No. 6, F-92260 Fontenay-aux-Roses (Seine), France
87. Theory Department Read File, c/o T. E. Stringer, JET Joint Undertaking, Abingdon, Oxfordshire OX14 3EA, United Kingdom
88. Theory Department Read File, c/o R. Briscoe, Culham Laboratory, Abingdon, Oxfordshire OX14 3DB, United Kingdom
89. Theory Department Read File, c/o D. Biskamp, Max-Planck-Institut für Plasmaphysik, Boltzmannstrasse 2, D-8046 Garching, Federal Republic of Germany
90. Theory Department Read File, c/o T. Takeda, Japan Atomic Energy Research Institute, Tokai Fusion Research Establishment, Tokai-mura, Naka-gun, Ibaraki-ken, Japan
91. Theory Department Read File, c/o J. Greene, General Atomics, P.O. Box 85608, San Diego, CA 92138
92. Theory Department Read File, c/o L. D. Pearlstein, L-630, Lawrence Livermore National Laboratory, P.O. Box 5511, Livermore, CA 94550
93. Theory Department Read File, c/o R. Gerwin, CTR Division, Los Alamos National Laboratory, P.O. Box 1663, Los Alamos, NM 87545
- 94-95. L. Garcia, Universidad Complutense, Madrid, Spain
96. H. Biglari, University of California-San Diego, La Jolla, CA 92093-0319
97. R. Bonomo, ECE Department, University of Wisconsin, 1415 Johnson Dr., Madison, WI 53706
98. C. P. T. Bussac, École Polytechnique, F-91120 Palaiseau, France
99. Z. Chang, Physics Department, University of Wisconsin, Madison, WI 53706
100. L. Chen, Princeton Plasma Physics Laboratory, P.O. Box 451, Princeton, NJ 08543

101. C. Z. Cheng, Princeton Plasma Physics Laboratory, P.O. Box 451, Princeton, NJ 08543
102. S. T. Chun, Courant Institute of Mathematical Sciences, New York University, 251 Mercer St., New York, NY 10012
103. J. W. Connor, Culham Laboratory, UKAEA, Abingdon, Oxon OX14 3DB, England
104. P. H. Diamond, University of California--San Diego, La Jolla, CA 92093-0319
105. K. Dimoff, INRS-Energie, C.P. 1020, Varennes, Quebec JOL 2PO, Canada
106. A. H. Glasser, CTR-6 Group, MS-F642, Los Alamos National Laboratory, P.O. Box 1663, Los Alamos, NM 87545
107. J. Greene, General Atomics, P.O. Box 85608, San Diego, CA 92138-5608
108. B. Guss, NW17-172, MIT Plasma Fusion Center, 175 Albany St., Cambridge, MA 02139
109. T. S. Hahm, Princeton Plasma Physics Laboratory, P.O. Box 451, Princeton, NJ 08543
110. R. J. Hastie, Culham Laboratory, UKAEA, Abingdon, Oxon OX14 3DB, England
111. T. C. Hender, Culham Laboratory, UKAEA, Abingdon, Oxon OX14 3DB, England
112. J. Johnson, Princeton Plasma Physics Laboratory, P.O. Box 451, Princeton, NJ 08543
113. S. K. Kim, Fusion Research Center, University of Texas, Austin, TX 78712
114. Y. B. Kim, University of California--San Diego, La Jolla, CA 92093-0319
115. Y. B. Kim, University of Wisconsin, Madison, WI 53706
116. M. Kotschenreuther, Institute for Fusion Studies, University of Texas, Austin, TX 78712
117. O. J. Kwon, University of California--San Diego, La Jolla, CA 92093-0319
118. C. S. Liu, Department of Physics and Astronomy, University of Maryland, College Park, MD 20742
119. S. Migliuolo, 26-205, Massachusetts Institute of Technology, Cambridge, MA 02139
120. F. Perkins, Princeton Plasma Physics Laboratory, P.O. Box 451, Princeton, NJ 08543
121. G. Rewoldt, Princeton Plasma Physics Laboratory, P.O. Box 451, Princeton, NJ 08543
122. K. S. Riedel, New York University, 251 Mercer St., New York, NY 10012
123. D. J. Sigmar, NW16-243, MIT Plasma Fusion Center, 167 Albany St., Cambridge, MA 02139
124. A. Sykes, Culham Laboratory, UKAEA, Abingdon, Oxon OX14 3DB, England

125. J. Weiland, Institute for Electromagnetic Field Theory and EURATOM-Fusion Research (SERC), Chalmers University of Technology, S-412 96 Göteborg, Sweden
- 126–171. Given distribution according to DOE/OSTI-4500, Energy Research (Distribution Category UC-427, Theoretical Plasma Physics)